Instruments and Experimental Techniques, Vol. 44, No. 4, 2001, pp. 455–461. Translated from Pribory i Tekhnika Eksperimenta, No. 4, 2001, pp. 38–44.

NUCLEAR EXPERIMENTAL TECHNIQUES

The Silicon Matrix as a Charge Detector for the ATIC Experiment

J. H. Adams, Jr[1]., G. L. Bashindzhagyan, V. I. Zatsepin, M. M. Merkin, M. I. Panasyuk, G. A. Samsonov, N. V. Sokol'skaya, and L. A. Khein

Skobeltsyn Institute of Nuclear Physics, Moscow State University, Vorob'evy gory, Moscow, 119899 Russia

Received October 3, 2000

Abstract—The characteristics of the silicon matrix which is the main charge detector in the ATIC balloon experiment are reported. The ATIC spectrometer was designed to measure the elemental composition and energy spectra of primary cosmic rays in an energy range of 10^{10} to 10^{13} eV with individual charge resolution from protons to iron under high albedo conditions from the calorimeter.

1. INTRODUCTION

The goal of the Advanced Thin Ionization Calorimeter (ATIC) experiment is to study the elemental composition and energy spectra of primary cosmic rays (PCR) in an energy range of 10^{10} to 10^{14} eV [1]. By now, a set of experiments in which an ionization calorimeter was used for direct measurements of PCR spectra from protons to iron have been performed. The pioneer experiments on board the PROTON-1, 2, 3 satellites (up to 10^{13} eV) and PROTON-4 (up to 10^{15} eV) were carried out in 1965–1968 [2, 3]. However, these measurements appeared to be unsuccessful due to the distortion of a signal in the charge detector by the albedo from the calorimeter. The next attempt was undertaken in 1972 in the balloon experiment by Ryan *et al.* [4]. An ionization calorimeter with scintillator charge detectors was exposed for 16 h at a depth of 6 g/cm^2. Four wire spark chambers determined the primary particle trajectory and cut events with backscattered particles. Only one flight was performed, and only proton and helium spectra were measured. The spectrometer was supposed to be exposed in the HEAO satellite for two years and collect data on all nuclei up to 10^{14} eV. However, this program was never realized. But, if realized, it hardly would have been successful, because the experimental scheme did not guarantee a satisfactory solution to the albedo problem. The experiments with emulsion calorimeters [5–7] also did not lead to irrefutable conclusions because of the high energy threshold, lack of statistics, and insufficient methodical reliability.

The SOKOL experiment (1984–1986) with a thick ($5.5\lambda_p$) ionization calorimeter was a successful one from the point of view of the experimental method [8, 9]. In this experiment, directional Cerenkov detectors were used to measure proton and helium charges, and they succeeded in eliminating the influence of backscattered particles and separating protons from helium nuclei. However, the charge resolution of the experiment was insufficient for individual resolution of heavier nuclei. Besides, the high energy threshold (2–5-TeV) and the limited exposure duration did not allow us to collect enough statistics to clear up some important questions and, chiefly, to solve the problem of the proton spectrum.

The ATIC experiment is a new attempt to measure the high-energy PCR spectra. In the experiment, the backscattering problem is solved through high segmentation of the charge detector.

The ATIC spectrometer consists of three main parts: the charge module, carbon target, and fully active BGO calorimeter (Fig. 1). In the experiment, the events selected are those in which a primary particle passes through the charge module, interacts in the target, and generates an electron-hadron cascade in the calorimeter. The charge is measured by a matrix of silicon detectors *1*. The target module consists of three layers of carbon *3* each 10 cm thick ($0.75\lambda_p$ totally) and three plastic-scintillator hodoscopes *2* with a cross section of 2×1 cm^2 and lengths of 88.2, 74.2, and 52.4 cm for the upper, lower, and middle hodoscope, respectively. Each hodoscope consists of two strip planes oriented at an angle of 90°. They help form the triggers determining the aperture of the instrument and provide additional measurements of the charge and trajectory of the primary particle. The calorimeter *4* consists of 400 crystals of bismuth germanate (BGO) $25 \times 2.5 \times 2.5$ cm^3 in size. The configuration of the instrument is described in more detail in [1, 10]. Questions on the simulation of cascades in the ATIC, i.e., energy resolution, primary particle trajectory reconstruction, charge resolution of the scintillator detectors are considered in [11, 12].

Here, we considered the characteristics of the silicon matrix, which is the new charge detector for high-energy cosmic rays.

[1] Naval Research Laboratory, Washington, P.C., USA

0020-4412/01/4404-0455$25.00 © 2001 MAIK "Nauka / Interperiodica"

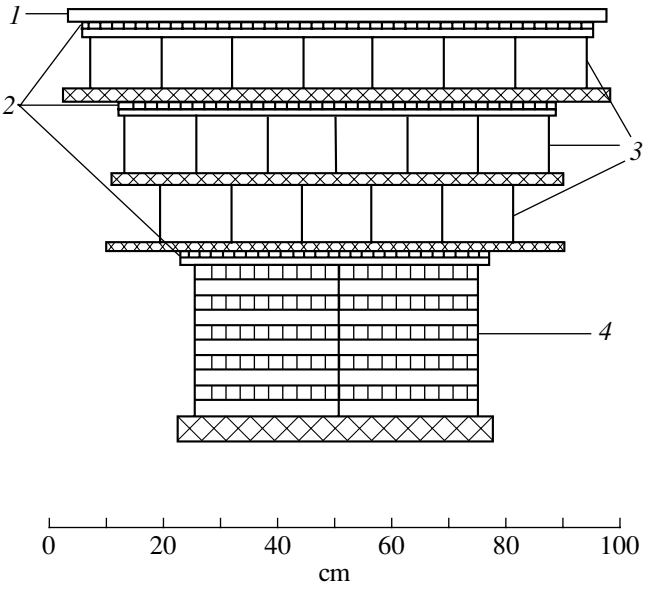

Fig. 1. The ATIC device: (*1*) silicon matrix; (*2*) scintillator detectors; (*3*) carbon target; and (*4*) ionization calorimeter.

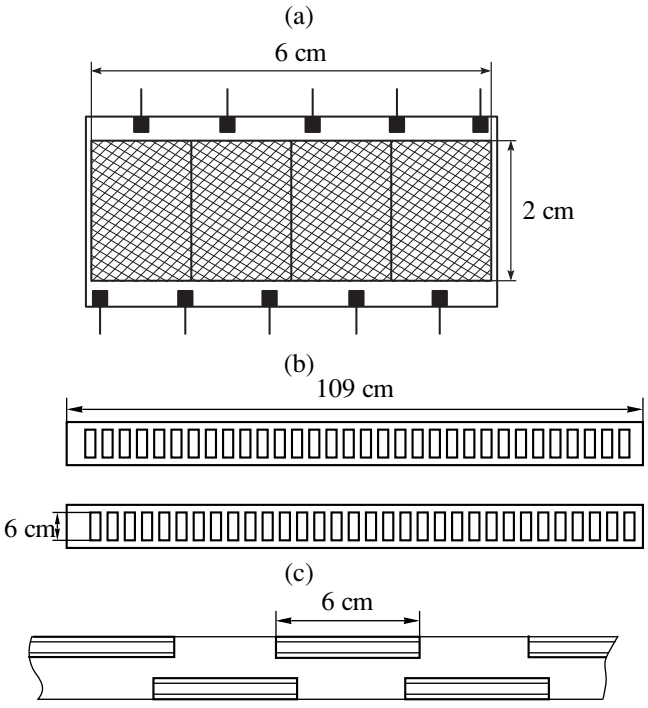

Fig. 2. Schematic of the silicon matrix: (a) daughterboard; (b) motherboards; and (c) ladders layout in the matrix.

2. SILICON MATRIX DESIGN

The silicon matrix designed for the ATIC experiment consists of 4480 silicon detectors arranged in four planes. The active detector areas in these planes partially overlap to cover completely the aperture. The smallest element of the matrix is a daughterboard with four electrically independent silicon detectors: pads (Fig. 2a). Twenty eight daughterboards are mounted on a motherboard (Fig. 2b), which is a multilayer circuit board 109 cm long and 6.634 cm wide that also carries the front-end electronics for the detectors. Two motherboards located one above the other "face to face" and shifted so that the active areas partially overlap form a structure termed a ladder. The matrix has two panels of ladders with 10 ladders in each that partially overlap. These panels are mounted with a shift, so that the active areas of the upper and lower ladders also partially overlap (Fig. 2c). The active area of the matrix is 99.2×111.2 cm^2.

The four-pad detectors are made on wafers of pure silicon 10 cm in diameter and 380 μm thick produced by Wacker Siltronic, Germany. Three four-pad detectors were made on each wafer. The active area of the detector pad is 1.945×1.475 cm^2, so that the whole detector has an active area of 1.945×5.9 cm^2.

The detector is a PIN diode with a sharp *p–n* junction. A common contact is created on one side by phosphorous diffusion, while the individual detector pads are produced on the other side by boron ion implantation. The nominal capacitance of each detector pad is 90 pF. The full depletion voltage for the selected detectors is <80 V, while the operating voltage is 100 V. The selected detectors are mounted on ceramic boards. The manufacturing techniques for the detectors are stated in more detail in [13].

3. ALBEDO SIMULATION

The simulation was performed for the initial version of the ATIC design with four carbon layers 10 cm thick and a layer of plexiglass 5 cm thick. The order of the layout and thickness of the layers from the top downward is given in Table 1 [10]. The simulation was performed using GEANT-3.21 package [14]. The hadronic cascade was simulated using the FLUKA package [15]. Proton was simulated as the primary particle for three energies: 100, 1000, and 10 000 GeV. Protons were incident isotropically on the upper plane of the ATIC. Only the protons that penetrated the silicon matrix along the trajectories that prolonged through the upper and bottom plane of the BGO calorimeter and interacted in the target section of the ATIC were accepted. The threshold energy was 0.1 MeV for photons and electrons in silicon and 1 MeV elsewhere, 0.2 MeV for hadrons in silicon and 2 MeV elsewhere. The number of events in the analysis was 30 000 for 100 GeV, 10 000 for 1000 GeV, and 1500 for 10 000 GeV.

Table 2 presents the mean number of albedo particles (per one cascade) of different kinds that produce an energy deposit anywhere in the silicon matrix above a certain value expressed in MIP: the mean energy deposited by a normally incident minimum ionizing particle. In the table, *electrons* mean electrons or positrons. It is

Table 1. ATIC configuration

Layer	Lateral size, cm	Thickness, cm
Silicon	100×100	0.038
Plexiglass	100×100	5.0
Scintillator	96.4×96.4	2.0
Carbon	96.4×96.4	10.0
Gap	96.4×96.4	2.0
Carbon	85.6×85.6	10.0
Gap	85.6×85.6	2.0
Scintillator	73.2×73.2	2.0
Carbon	73.2×73.2	10.0
Gap	73.2×73.2	2.0
Carbon	62.4×62.4	10.0
Gap	62.4×62.4	2.0
Scintillator	50.0×50.0	2.0
BGO	50.0×50.0	25.0

clear that the main contribution comes from electrons, pions, and photons. The energy dependence of the albedo signal has approximately a power form with the maximum rate for photons ($\sim E^{0.65}$) and with a lower rate for electrons ($E^{0.53}$) and for charged hadrons ($E^{0.4}$).

The following computing was done for a silicon matrix with cells of 3×3 cm^2. Table 3 presents the probability of events where the signal of the albedo particles exceeds a certain value in the axial cell through which the primary proton enters. Because of the uncertainty about the primary particle location in the matrix, the signals from neighboring (to the axial) cells should be taken into account in addition to that from the axial one.

Table 4 presents the probability of misidentification of a proton as a helium nuclei when some signals exist in the neighboring cells. To calculate these values, it is assumed that a proton is misidentified as a helium nuclei if the sum of the signal from the primary particle in the axis cell and the albedo signal in the axial cell or in any neighboring cell in the "circle of confusion" is higher than 3 MIP.

The reconstruction of the location of the proton entering the silicon matrix showed [11] that the rms of the coordinate reconstruction σ depends on the energy and is 4.6 cm for 100 GeV, 1.95 cm for 1000 GeV, and 1 cm for 10 000 GeV. If we were to accept that the radius of the "circle of confusion" is 3σ, it follows from Table 4 that the probability of misidentifying a proton as a helium nucleus because of albedo is 1.9%, 1.4%, and 1.4% for the energies 100, 1000, and 10 000 GeV, respectively. Note that this probability is small and does not increase with an energy increasing 100 times.

The computing of albedo was performed at the stage of the ATIC design. In the final configuration one layer of the carbon target was removed, resulting in a certain increase in the effect of albedo particles on the silicon matrix; on the other hand, the size of the silicon cell was decreased to 1.5×2 cm instead of 3×3 cm in the simulation. The estimations made make possible to

Table 2. Mean number of albedo particles that produce a signal in the silicon matrix above a given value

Particles	A, MIP				
	$\geq > 0$	> 1	> 2	> 3	> 4
	$E = 10^2$ GeV				
Electron	0.688	0.569	0.196	0.093	0.051
Pion	0.151	0.136	0.057	0.025	0.013
Proton	0.015	0.015	0.015	0.014	0.013
Photon	0.174	0.053	0.021	0.011	0.007
Neutron	0.001	0.000	0.000	0.000	0.000
	$E = 10^3$ GeV				
Electron	2.179	1.795	0.611	0.301	0.170
Pion	0.355	0.308	0.121	0.052	0.026
Proton	0.050	0.050	0.049	0.046	0.043
Photon	0.590	0.191	0.081	0.041	0.025
Neutron	0.003	0.001	0.001	0.001	0.000
	$E = 10^4$ GeV				
Electron	7.639	6.268	2.118	1.066	0.588
Pion	1.060	0.915	0.293	0.123	0.062
Proton	0.195	0.195	0.191	0.177	0.165
Photon	2.354	0.740	0.319	0.155	0.945
Neutron	0.015	0.004	0.004	0.002	0.002

Table 3. Probability of events in which the signal of albedo particle in the axial cell exceeds a certain value

E, GeV	Signal value in the axial cell, %				
	> 0	> 1	> 2	> 3	> 4
10^2	0.42	0.25	0.10	0.04	0.02
10^3	0.82	0.52	0.20	0.10	0.06
10^4	2.21	1.46	0.67	0.25	0.14

Table 4. Probability of misidentification of a proton as a helium nuclei in the presence of albedo signals in neighboring cells

E, GeV	Radius of the confusion circle, cm		
	3	9	15
10^2	1.00	1.30	1.89
10^3	1.09	1.87	3.26
10^4	1.37	3.23	7.07

Table 5. Number of Daughterboards with a given value of noise (σ)

	σ, MIP					
	<0.15	0.15–0.3	0.3–0.45	0.45–0.6	0.6–0.75	>0.75
Number of daughterboards	804	382	49	37	20	213
Fraction of the total number of daughterboards, %	53.4	25.4	3.2	2.4	1.3	14.2

accept the above results as a good approximation of the actual situation in the ATIC instrument and to conclude that the silicon matrix allows reliable resolution of protons and helium nuclei in the entire accessible energy region.

4. CHARACTERISTICS OF SILICON DETECTORS

The characteristics of silicon detectors were studied on a laboratory setup. The response of silicon detectors to the passage of a single charged relativistic particle was measured. For this purpose, electrons from a ^{90}Sr radioactive source with energies of 1.5 to 2.2 MeV were used. The nonrelativistic component of the β-spectrum (E < 1.5 MeV) was clipped by an aluminium filter. The inherent noise of detectors was measured using a pulser gauge peak width as a difference between the measured total noise of the detector plus the preamplifier and the noise of the preamplifier itself. The amplifier noise measurement was performed with an equivalent capacitor replacing the detector.

To check that the measured noise of the detector in fact determines the widening of the energy deposition distribution, the measured spectra were compared with the results of the simulation.

The detector response was simulated by using GEANT-3.21 for electrons with an energy of 2 MeV. The inherent noises of the detector and electronics were added in the calculation as a random variable distributed under the normal law with a variance measured by the calibration signal spreading. Figure 3 shows a comparison between the simulated signal distribution for a detector and electronics noise equal to 0.11 MIP and the experimental one. The simulations for detectors with different inherent noise levels show that the width of experimental signal distribution is well described properly by the simulation, indicating the accuracy of the measurements of the detector noise characteristics.

By now, the noises of more than 6000 individual detectors made for the ATIC experiment have been measured. Table 5 shows the numbers of daughterboards with a given value of σ(σ is expressed in MIP). The σ value in the table refers to the worst detector of the daughterboard.

A typical value of the noise is σ ~ 0.05 MIP, while the greater bulk of detectors has an inherent noise at a level of <0.3 MIP, allowing, as will be shown below, reliable resolution of protons and helium. Such detectors are selected for the matrix. For nuclei heavier than helium, the influence of the detector noise is negligibly small.

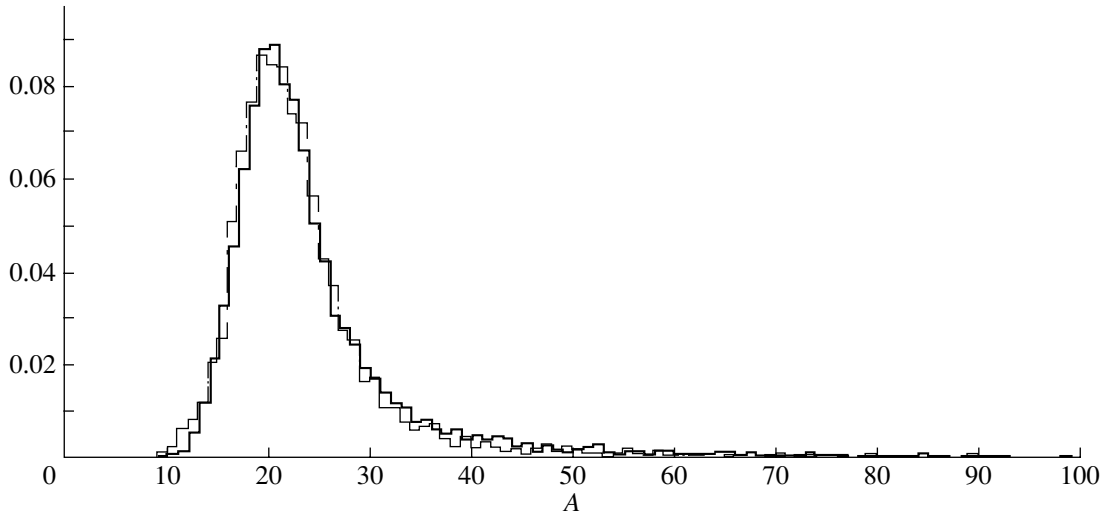

Fig. 3. Simulated (solid line) and experimental (dashed line) distributions of the ionization signal from a singly charged particle: *A* is the channel number (1 MIP corresponds to *A* = 21).

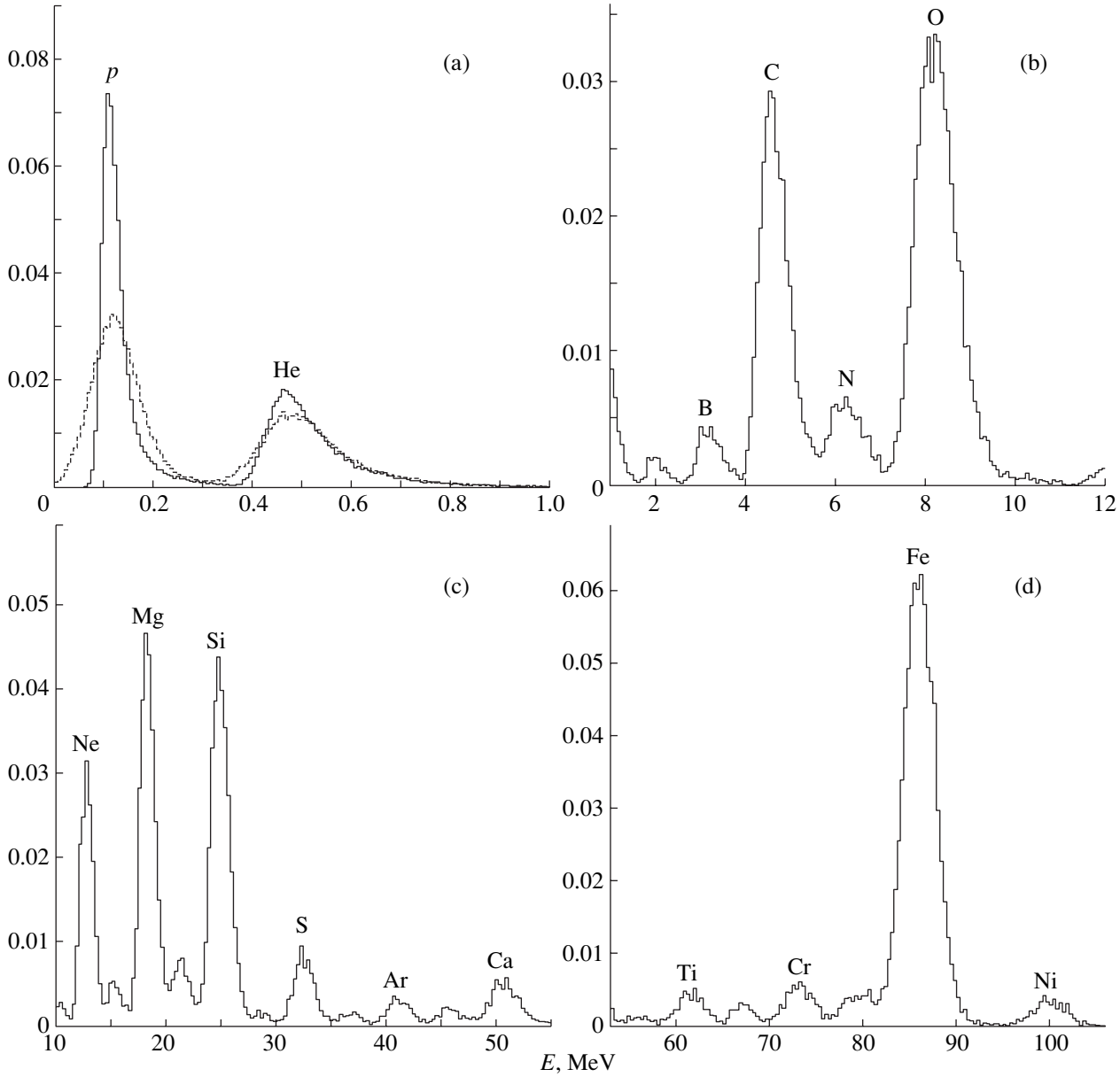

Fig. 4. Distributions in the energy released in the detector for various nuclei: (a) protons and helium nuclei; (b) helium–neon; (c) fluorine–calcium; and (d) scandium–nickel. The noise levels are 7 (solid curves) and 40 keV (dashed curves).

Another factor that influences the silicon charge detector resolution is the nonuniformity of the silicon disk thickness. According to the manufacturer, the deviation of the average thickness of silicon from disk to disk can reach ~5%. However, the deviation of the average signal values of individual detectors can be taken into account in the analysis of experimental data. Only the contribution of the internal thickness nonuniformity of the detector is ineradicable.

The experimental estimation of the thickness nonuniformity for a cell of 1.5×2 cm yields an rms deviation of ~1%.

5. SIMULATION OF THE DETECTOR RESPONSE TO THE PASSAGE OF A NUCLEUS WITH CHARGE Z

The response of the silicon detector was simulated using GEANT-3.21 with the assumption that the passage of a nucleus with the charge Z is equivalent, from the point of view of ionization losses, to the passage of Z^2 protons with energies equal to the energy per nucleon of the given nucleus (although in the used version of GEANT the ionization losses for nuclei are included, the fluctuations of these losses are described incorrectly). The calculation is made for vertically passing nuclei with an energy of 200 GeV per nucleus.

Table 6. Cosmic ray nuclei abundance

Z	*A*	*N*
1	1	50999
2	4	35307
3	7	300
4	9	291
5	10	764
6	12	6045
7	14	1628
8	16	10000
9	19	178
10	20	2199
11	23	413
12	24	3819
13	27	711
14	28	4292
15	31	153
16	32	946
17	35	175
18	40	420
19	39	275
20	40	788
21	45	146
22	48	580
23	51	339
24	52	778
25	55	649
26	56	9322
27	59	48
28	59	557

The number of nuclei of each type is taken from data on the charge composition of the HEAO-3 experiment at E = 16 GeV/nucleon [16] and from the SOKOL experiment at E = 2.5 TeV [9] (see Table 6).

Figure 4a shows the distribution of the energy deposition in the detector for protons and helium; the normal distribution of the noise with variances of 0.05 MIP (~7 keV, solid line) and 0.3 MIP (~40 keV, dashed line) is added to the distribution of the ionization losses. One can see, that a larger number of detectors (according to Table 5) reliably discriminate between protons and helium nuclei.

The distribution from helium to neon is shown on Fig. 4b. In this region of energy deposition, the contribution of the detector noise is negligibly small (the calculation was done for σ_n = 7 keV). Figures 4c and 4d show the ranges from fluorine to calcium and from scandium to nickel, respectively.

The detector response spreading caused by the nonuniformity of the detector thickness was taken into account for all calculated distributions as well. In each figure, the area under the curve is normalized to unity.

For nuclei heavier than carbon, the shape of the ionization loss distribution is close to Gaussian, and, thus, the resolution may be described by the expression

$$\delta_A^2 = \delta_i^2 + \delta_n^2 + \delta_{th}^2,$$

where $\delta_A = \sigma_A/A$ is a relative deviation of the signal value ($A \sim Z^2$), δ_i, δ_n, and δ_{th} are the contributions of ionization fluctuations, detector noise, and thickness nonuniformity, respectively. With the detectors' parameters described above, this expression is written as follows:

$$\delta_A^2 = (0.44/Z)^2 + (0.05/Z^2)^2 + (0.01)^2.$$

The relative standard deviation of the charge value $\delta_Z \cong \delta_A/2$ gives a charge resolution σ_Z = 0.22–0.26 charge units from carbon to iron. In this value, the contribution of the ionization fluctuations dominates for all charges and becomes comparable with the contribution of the thickness nonuniformity for the iron group.

CONCLUSION

The highly segmented silicon matrix is for the first time applied to charge measurements in the field of high-energy primary cosmic rays. Its application ensures individual charge resolution of cosmic ray nuclei from protons to iron under conditions of high albedo from an ionization calorimeter.

ACKNOWLEDGMENTS

This work was performed for the ATIC Collaboration and was supported by the Russian Ministry of Science and Technology and Russian Foundation for Basic Research, project no. 99-02-16246.

REFERENCES

1. Guzik, T.G. *et al.*, Abstracts of Papers, *26 Int. Cosmic Ray Conf., Salt Lake City*, 1999, vol. 5, p. 9.
2. Grigorov, N.L., Kakhidze, G.P., Rapoport, I.D., *et al.*, *Kosm. Issled.*, 1967, vol. 5, p. 383.
3. Grigorov, N.L., Mamontova, N.A., Rapoport, I.D., *et al.*, Abstracts of Papers, *12 Int. Cosmic Ray Conf.,* Tasmania, 1971, vol. 5, p. 1752.
4. Ryan, M.G., Ormes, J.F., Balasubramanyan, V.K., *et al.*, *Phys. Rev. Lett.*, 1972, vol. 28, p. 985.
5. Cherry, M.L. *et al.*, Abstracts of Papers, *25 Int. Cosmic Ray Conf.*, Durban, 1997, vol. 4, p. 1.
6. Zatsepin, V.I., Zamchalova, E.A., Varkovitskaya, A.Ya., *et al.*, Abstracts of Papers, *23 Int. Cosmic Ray Conf.*, Calgary, 1993, vol. 2, p. 13.

7. Apanasenko, A.V., Beresovskaya, V.K., Fujii, M., *et al.*, Abstracts of Papers, *26 Int. Cosmic Ray Conf.*, Salt Lake City, 1999, vol. 3, p. 163.
8. Grigorov, N.L., *Yad. Fiz.*, 1990, vol. 51, no. 1, p. 157.
9. Ivanenko, I.P., Shestoperov, V.Ya., Chikova, L.O., *et al.*, Abstracts of Papers, *23 Int. Cosmic Ray Conf.*, Calgary, 1993, vol. 2, p. 17.
10. Guzik, T.G., Adams, J.H., Bashindzhagyan, G.L., *et al.*, Abstracts of Papers, *SPIE Int. Symp. on Optical Science, Engineering, and Instrumentation*, Denver, 1996, vol. 2806, p. 122.
11. Seo, E.S., Adams, J.H., Bashindzhagyan, G.L., *et al.*, Abstracts of Papers, *SPIE Int. Symp. on Optical Science, Engineering and Instrumentation*, Denver, 1996, vol. 2806, p. 134.
12. Wang, J.Z., Seo, E.S., Adams, J.H., *et al.*, Abstracts of Papers, *25 Int. Cosmic Ray Conf.*, Durban, 1997, vol. 5, p. 5.
13. Baranova, N.V., Bashindzhagyan, G.L., Voronin, A.G., *et al.*, *Preprint of Res. Inst. of Nucl. Phys. of Moscow State Univer.*, Moscow, 1995, no. 95-43/407.
14. Brun, R., Bruyant, F., Maire, M., *et al.*, *GEANT Users Manual*, CERN DD/EE/84-1, Geneva, 1984.
15. Arino, P.A., *Fluka User's Guide*, TIS-RP-190, CERN, 1987.
16. Engelmann, J.J., Ferrando, F., Soutoul, A., *et al.*, *Astron. Astrophys.*, 1990, vol. 233, p. 96.
17. The ATIC Collaboration, Abstracts of Papers, *26 Int. Cosmic Ray Conf.*, Salt Lake City, 1999, vol. 7, p. 433.